Temperature dependence of the superconducting gap of single-layer FeSe/SrTiO₃: Direct comparison between transport and spectroscopic measurements

Koshiro Ide,[*] Tomoaki Tanaka,[*,†] Asger Pedersen [ORCID],[‡] Satoru Ichinokura [ORCID], and Toru Hirahara [ORCID][§]

Department of Physics, Tokyo Institute of Technology, Tokyo 152-8551, Japan

We studied the superconducting properties of the one-unit cell FeSe grown on high-doped SrTiO₃(001) (STO) substrate by *in situ* transport and angle-resolved photoemission spectroscopy (ARPES) measurements. By comparing with previous data taken for the low-doped STO substrate [Phys. Rev. Lett. **124**, 227002 (2020)], it was revealed that the onset of superconductivity occurs at ∼40 K irrespective of the STO doping level. Furthermore, from the temperature dependence of the critical current, we were able to deduce the superconducting gap that is relevant in the transport phenomena, which gradually increases by cooling the sample down from 40 K. In contrast, the coherent peak emerges at 60 K that likely corresponds to the Cooper pair formation, while the leading edge shift near the Fermi level is clearly observed at 40 K in the ARPES spectra. We speculate that the STO surface presumably acts as an effective "disorder" in this system and the Cooper pairs are preformed well above the onset of the resistance drop.

I. INTRODUCTION

Superconductivity in two-dimensional (2D) materials has attracted interest for a long time. Nowadays, not only the classical granular or amorphous films [1,2] but atomically thin single-crystalline films [3–5] have been found to show superconductivity and their exotic properties are discussed in terms of quantum phase transition [6,7] or the effect of the spin-orbit coupling [8,9]. In general, the transition temperature (T_c) of 2D superconductors is low. However, monolayer (single unit cell, 1UC) FeSe grown on SrTiO₃(001) surface (STO) has been under intense investigation since the T_c was reported to be over 40 K, which is much higher than that of the bulk (∼8 K). Although the importance of the FeSe/STO interface has been recognized, the reported value of T_c varies greatly between different reports. *In situ* four-point-probe (4PP) measurements that characterize the intrinsic transport properties have not even reached the same conclusion. Whereas the initial report on 1UC FeSe/high-doped STO reported $T_c \sim$ 109 K [10], the following reports using low-doped substrates only showed a T_c^{onset} of 40 K as well as zero resistance at $T_0 \sim$ 15–30 K [11,12]. The latter was consistent with the results of *ex situ* transport measurements [13]. Furthermore, Ref. [12] showed from *in situ* angle-resolved photoemission spectroscopy (ARPES) measurements on the same sample that the gap in the ARPES spectra can be observed above

T_c^{onset} up to 60 K, suggesting the presence of pseudogap states where the Cooper pairs are likely formed but are incoherent.

As such, the exceptionally high $T_c \sim$ 109 K reported on 1UC FeSe/high-doped STO substrate [10] needs further verification. Furthermore, the relation between the transport data and the evolution of the gap in spectroscopic studies should be examined. Thus, in the present study, we aimed to clarify these aspects and performed *in situ* 4PP transport and ARPES measurements on the same 1UC FeSe film grown on a high-doped STO substrate. By comparing with our previous results for the sample formed on low-doped STO [11], we found that the T_c of the 1UC FeSe/STO does not depend on the substrate doping level ($T_c^{\text{onset}} \sim$ 40 K). By focusing on the temperature dependence of the critical current, we deduced the temperature dependence of the macroscopic superconducting gap that is relevant to charge transport. It showed a monotonic increase from T_c^{onset}. In contrast, the coherence peak emerged at 60 K, whereas the leading edge shift near the Fermi level shows a prominent change at 40 K in ARPES. This likely shows the presence of preformed Cooper pairs due to the STO surface potential which effectively acts as "disorder." Our results point to the importance of correctly identifying the meaning of the measured "energy gap" in each experimental method.

II. EXPERIMENT

A commercially available Nb-doped SrTiO₃(001) (0.5 wt. %, Shinkosha) was used as the substrate. After degassing at 500 °C in ultrahigh vacuum overnight, the samples were etched under Se flux at 950 °C for 30 min [14]. Further annealing without flux at 700 °C for 30 min completes the formation of the atomically ultraclean surface of STO evidenced by the sharp $\sqrt{13} \times \sqrt{13}$ patterns in the reflection high-energy electron diffraction (RHEED), as shown in Fig. 1(a). The 1UC FeSe was formed by codepositing Fe

---

[*]These authors contributed equally to this work.

[†]Present address: National Institutes for Quantum Science and Technology, Takasaki, Gunma 370-1292, Japan.

[‡]Present address: Department of Physics, Technical University of Denmark, Lyngby 2800 Kgs, Denmark.
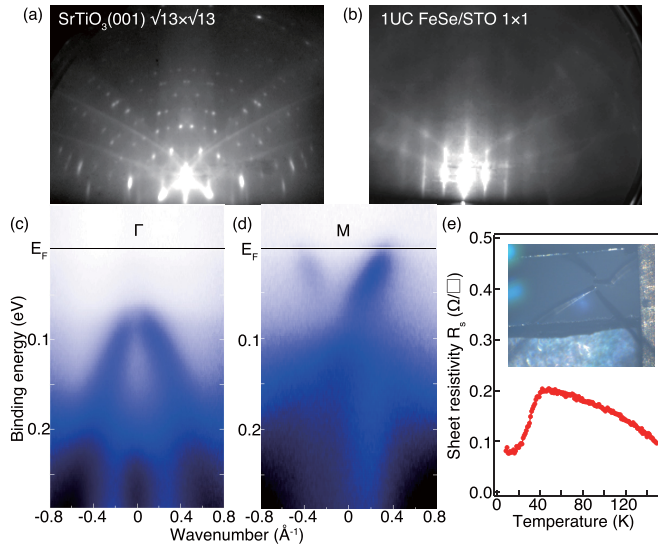
[§]hirahara@phys.titech.ac.jp

FIG. 1. (a) RHEED pattern of the SrTiO$_3$(001) $\sqrt{13} \times \sqrt{13}$ surface after cleaning the high-doped wafer in UHV. (b) RHEED pattern of 1UC FeSe after film growth on the high-doped STO substrate. (c) Band dispersion of the 1UC FeSe film grown on the high-doped STO at the Γ point, showing the hole band below E_F. The measurement was performed at 25 K. (d) Band dispersion of the 1UC FeSe film grown on the high-doped STO at the M point, showing the electron pocket at E_F. The measurement was performed at 60 K. (e) Temperature dependence of the sheet resistivity R_s for the 1UC FeSe film grown on the high-doped STO. The inset shows the actual probe configuration.

(99.5%) and Se (99.999%) with a flux ratio of 1 : 10 with the substrate temperature at 400 °C. The RHEED oscillation was used to determine the film thickness. The grown films were postannealed at 450–570 °C by gradually increasing the temperature for 30 min. The band structure was measured in each step to ensure the optimum annealing condition that shows the proper doping level for the occurrence of superconductivity as shown in Fig. S1 [15]. The high quality of the grown film is assured also from the RHEED pattern shown in Fig. 1(b).

ARPES measurements were performed *in situ* after the sample preparation with a commercial hemispherical photoelectron spectrometer equipped with angle and energy multidetections (ScientaOmicron R4000) with He Iα radiation (21.2 eV) at 25–90 K. The energy resolution was set to ∼10 meV. The Fermi level was determined by measuring the Ta plate of the sample holder fixing the STO substrate as shown in Fig. S2 [15].

Transport measurements were performed *in situ* after the ARPES measurements. The system has four probes which can move independently and by touching the surface of the sample, 4PP resistance measurements can be performed in UHV [inset of Fig. 1(e)] [11]. The measurements were performed down to 8 K in the present experiment. We employ the dual-configuration method near zero bias to deduce the sheet resistivity R_s and the $I-V$ curves shown are those for the R_a configuration [11,16].

III. RESULTS AND DISCUSSION

Figures 1(a) and 1(b) show the RHEED patterns of the STO substrate with the $\sqrt{13} \times \sqrt{13}$ periodicity (a) and the grown 1UC FeSe film (b), respectively. One should note that the features of the RHEED pattern are similar to those for the nondoped substrate sample reported in Ref. [11]. Thus one can be sure that the sample quality does not depend on the STO substrate.

An advantage to using the high-doped STO substrate is that low-temperature ARPES measurements are possible. We have performed ARPES measurements as shown in Fig. S1 to obtain the optimum annealing condition [15]. Figures 1(c) and 1(d) show the band dispersion images of the 1UC FeSe film at the Γ (c) and M (d) points after the optimum annealing, respectively. The well-known hole band at Γ and electron pocket at M for the superconducting 1UC FeSe can be recognized [17,18]. Note that Fig. 1(d) was taken at 60 K and is showing some intensity at the Fermi level as discussed in detail below. This also reassures one that the films we have grown are of high-quality and there are no regions in the sample where the film thickness exceeds 1UC [18,19]. The energy of the top of the hole band at the Γ point, the energy of the bottom of the electron pocket, and the Fermi wave number are all nearly the same as the data in the literature for the optimally annealed 1UC FeSe/STO [12,17,19]. Thus one can be sure that the electron doping level in the present system is maximized to verify the highest possible T_c in this system.

In contrast, 4PP resistance measurements become difficult on samples formed on the high-doped STO since the substrate itself becomes conductive. However, we were able to measure such low resistance and the temperature (T) dependence of the 2D sheet resistivity (R_s) is shown in Fig. 1(e). Figure 2(a) shows the comparison between the present sample and that for the low-doped substrate reported in Ref. [11]. Note that the values of R_s for the present sample are in the order or 0.1 Ω, which is 10 000 times smaller than the values for the low-doped STO wafer. Thus the STO substrate contribution is included in the present experiment, which is reflected in the difference of the T-dependent behavior for the two samples above ∼40 K in Fig. 2(a). In contrast, one can notice a sudden drop of R_s below ∼40 K for both samples. Namely, R_s drops from 2 kΩ at 44 K to 20 Ω (nearly zero compared to the normal resistance) at $T_0 \sim 13$ K, while R_s decreases from 0.2 Ω at 38 K to 0.08 Ω at $T \sim 15$ K. The behavior of the 1UC FeSe grown on the low-doped substrate was unambiguously assigned as a superconducting transition [11], similar to other works [12–14]. Thus, although a clear zero resistance was not detected for the 1UC FeSe grown on the high-doped STO due to the substrate contribution, it can be said that the sudden drop at 38 K corresponds to the occurrence of superconductivity. This shows that the superconducting transition of the 1UC FeSe/STO system occurs universally at the onset temperature T_c^{onset} of ∼40 K, irrespective of the STO substrate.

Evidence of the occurrence of superconductivity can also be found in the $I-V$ curves as shown in Figs. 2(b) and 2(c). While the $I-V$ curves for the normal state above T_c^{onset} show a linear behavior [Fig. 2(b)], it becomes nonlinear at 15 K [Fig. 2(c)]. This behavior is also universal irrespective of the STO doping level. Note that $I-V$ characteristics
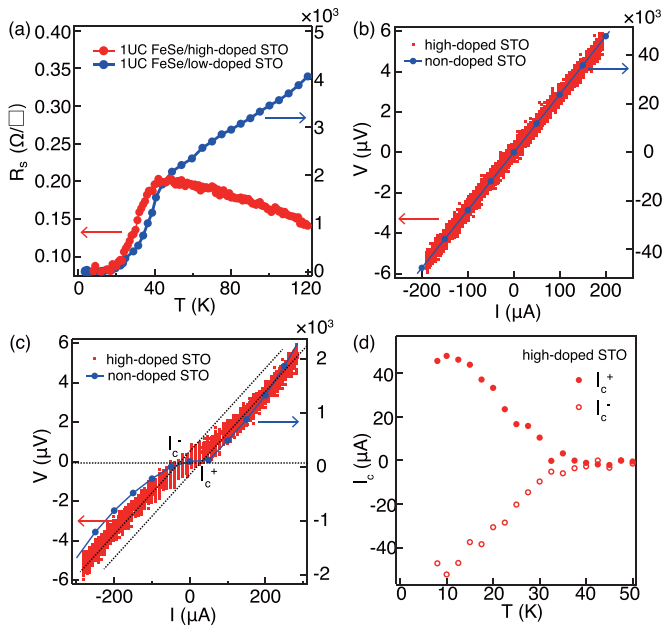
FIG. 2. (a) Temperature dependence of the sheet resistivity R_s for the 1UC FeSe film grown on the high-doped STO (red) shown together with that for the 1UC FeSe film grown on the nondoped STO (blue) reported in Ref. [11]. (b) $I - V$ characteristics at 45 K for the 1UC FeSe grown on the high-doped (red) and nondoped (blue) STO substrates. Both are linear and reflect the nonsuperconducting character. (c) $I - V$ characteristics at 15 K for the 1UC FeSe grown on the high-doped (red) and nondoped (blue) STO substrates. Both are nonlinear and reflect the superconducting character. The critical current $I_c^{\pm}$ is defined at the point where the straight line extracted from nonsuperconducting sides crosses the abscissa. (d) Extracted $I_c^{\pm}$ plotted as a function of the temperature for the 1UC FeSe film grown on the high-doped STO.

obtained by point probes do not show a jump from zero voltage to ohmic behavior typical for a superconductor. Since the current spreads radially from the drain probe in the present setup, the current density is not uniform and decreases as the distance from the drain probe becomes larger. Thus the broken superconductivity is gradually recovered when the voltage probe is placed far from the drain probe and this results in the blunt transition we have observed in our $I - V$ curves [11]. Still, it is possible to distinguish the nonlinear one from the linear one and extract the "critical current" $I_c^{\pm}$, where the superconductivity breaks due to the large current. It is defined at the point where a straight line extracted from nonsuperconducting sides crosses the abscissa, as shown in Fig. 2(c). The temperature dependence of I_c^+ and I_c^- for the present sample is shown in Fig. 2(d) and the occurrence of nonlinearity at 38 K is consistent with the $T_c^{\rm onset} = 38$ K as discussed above. Thus these two important findings from *in situ* 4PP transport measurements show that the onset of superconductivity of 1UC FeSe/STO does not depend on the substrate doping level. This is natural considering that the doping at the interface is presumably the main factor for the high-T_c in this system. Taking into account the results of Ref. [12], which also show this tendency, we speculate that $T_c \sim 109$ K reported for 1UC FeSe/high-doped STO substrate

in Ref. [10] detected something that was not really relevant to the superconductivity.

Let us further examine this temperature dependence of $I_c^{\pm}$. Generally superconductivity is broken by applying large current since the Cooper pairs acquire enough energy to overcome the pairing strength. The latter roughly corresponds to the superconducting gap size and it can be said that the temperature dependence of $I_c^{\pm}$ shown in Fig. 2(d) contains information on the gap. For a quantitative analysis, we refer to Ref. [4], where it was discussed that the atomic steps are the dominant source of electrons scattering for atomically thin superconducting films. The steps serve as Josephson junctions and the temperature dependence of the critical current $I_c(T)$ is given by the following equation [20]:

$$I_c(T) \propto \frac{\pi \Delta(T)}{2eR_{\rm step}} \tanh \frac{\Delta(T)}{2k_B T}, \qquad (1)$$

where $\Delta(T)$ is the temperature-dependent superconducting gap, $R_{\rm step}$ is the temperature-independent step resistance, e is the elementary charge, and k_B is the Boltzmann constant. It should be noted that $\Delta(T)$ in Eq. (1) is the gap related to the transport phenomena which is the ensemble average of the superconducting gap within the spatial distribution of the current.

As discussed above, since the $I_c^{\pm}$ derived from the present experiment is not the actual critical current, it is impossible to deduce the actual value of $\Delta(T)$ from the data in Fig. 2(d). However, it is possible to derive the relative change of the superconducting gap size as a function of temperature [$\Delta(T)$] by numerically solving Eq. (1) self-consistently using the experimental data $I_c^{\pm}$. The result is shown in Fig. 4. We have normalized the obtained values with the value obtained at the lowest measurement temperature. Similar analysis was performed for the temperature dependence of $I_c^{\pm}$ for the sample grown on the low-doped STO shown in Fig. 3(d) of Ref. [11]. The same trend can be found for the 1UC FeSe grown on both high-doped and low-doped STO substrates. Thus the transport data shows that the Δ develops from $T_c^{\rm onset}$ and becomes larger as the temperature is decreased.

We compare the data obtained with 4PP with the ARPES data. It is well known that ARPES is suitable to characterize $\Delta(T)$ [12,17,19]. Figure 3(a) shows the electron pocket at M for the 1UC FeSe/high-doped STO measured at 25 K. In contrast to Fig. 1(d), a gap has emerged as well as a band fold back, which can be recognized in the second derivative image of Fig. 3(b). For a quantitative analysis, we show in Fig. 3(c) the energy distribution curve (EDC) at the Fermi wave number k_F for the data at different temperatures (25–90 K). Although it is not clearly resolved in Fig. 3(a), there are actually two electron pockets as has been reported in Ref. [21]. We will focus on the outer band and adopt $k = 0.25$ Å^{-1} in our analysis [white lines in Figs. 3(a) and 3(b)] since it has been reported that for smaller k, the mixture of the inner and outer band does not give the correct physical picture [21]. The analysis for this kind of situation ($k = 0.2$ Å^{-1}) can be found in Fig. S3 [15].

Figure 3(d) shows a closeup of the features near E_F with the intensity normalized with that at the peak position to show the shift in the leading edge. The energies where the spectral peak becomes half in intensity has been analyzed [22] and one can clearly notice that the energy position shows a prominent
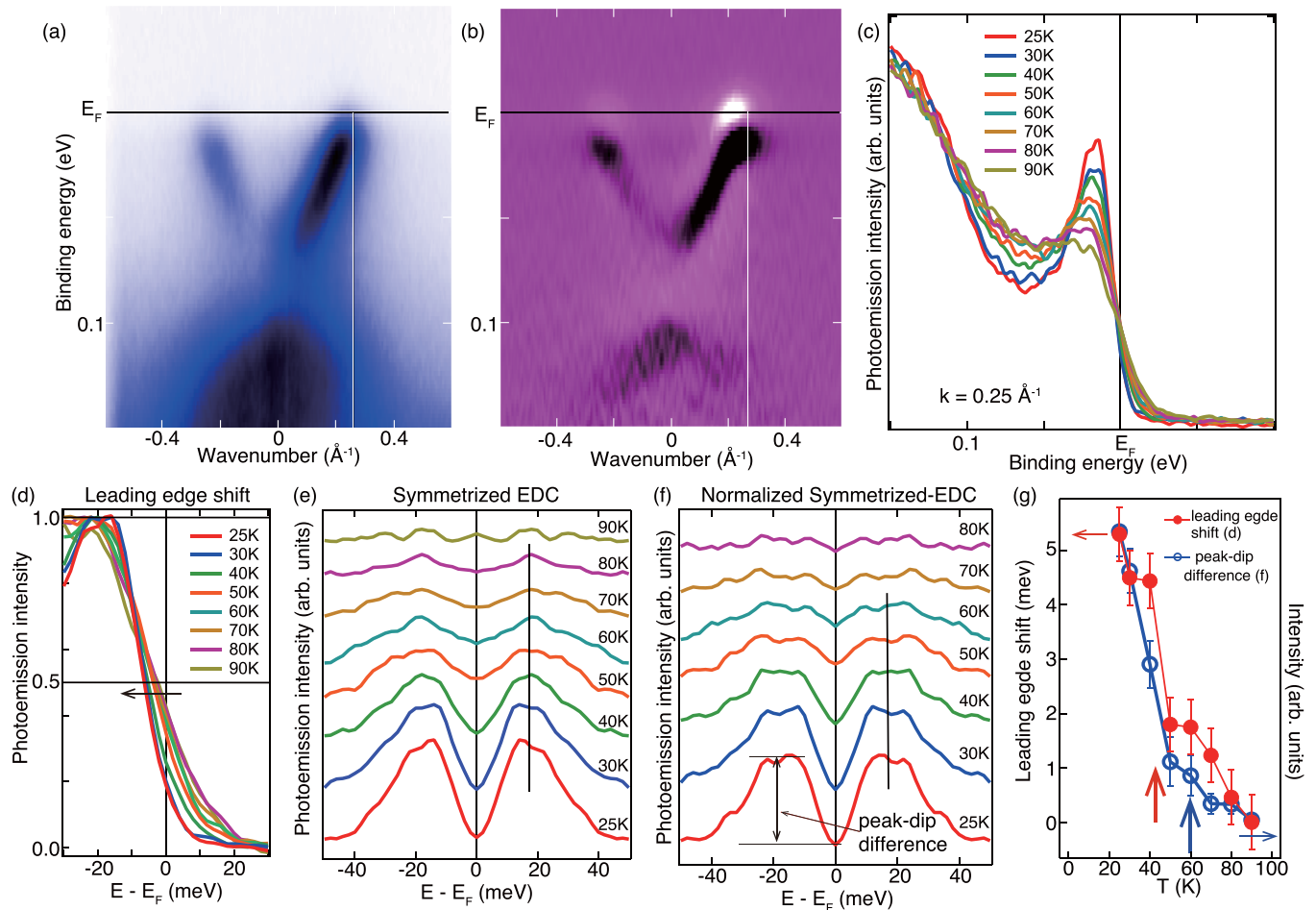
FIG. 3. (a) Band dispersion of the 1UC FeSe film grown on the high-doped STO at the M point, showing the electron pocket at E_F measured at 25 K. (b) Second derivative of the data shown in (a) to enhance spectral features. (c) Temperature dependence EDC curves at k_F near the M point taken from the band dispersion images such as the one shown in Fig. 1(d) for the 1UC FeSe film grown on the high-doped STO. The EDC spectra were taken at the cut indicated by the white lines in (a) and (b). (d) Same as (c) but with the intensity normalized with that at the peak position to show the shift in the leading edge. The energies where the spectral peak becomes half in intensity has been analyzed. (e) Temperature dependence of the symmetrized EDC from the data as shown in (c), indicating the gaplike feature for the data below 80 K and a metallic one for that at 90 K. (f) Normalized symmetrized EDC derived by dividing the symmetrized EDC with that of 90 K to enhance the features of superconductivity. The coherence peak likely emerges from 60 K. (g) Quantitative analyses of the leading edge shift shown in (d) and the peak-dip difference of the spectra shown in (f). The two distinct analyses likely give different temperatures concerning the onset of superconductivity.

change for the spectra of 40, 30, and 25 K compared to the others by 4–5 meV. Thus we can say that superconductivity is occurring between 40 and 50 K. Another signature of superconductivity in ARPES can be found in the Bogoliubov peak near E_F and it seems to be sharpening as the temperature is lowered. To exclude the effect of the Fermi-Dirac distribution, the symmetrized EDCs are shown in Fig. 3(e). It seems that the quasiparticle coherence peaks are present at 80 K and its position is nearly temperature independent ($\sim$17 meV). At 90 K, the symmetrized EDC seems to be metallic and, following Ref. [21], we have normalized the symmetrized EDCs with that of 90 K to emphasize the features of the coherent peaks, as shown in Fig. 3(f). One can now see that the spectra at 70 and 80 K do not show a clear indication of the coherent peak. For a quantitative discussion of the above EDC analyses, we have plotted in Fig. 3(g) the leading edge shift in Fig. 3(d) and the peak-dip difference in Fig. 3(f). It clearly shows that

the two distinct analyses give different temperatures concerning the onset of superconductivity. Overall, we can say that the ARPES data are mostly consistent with previous reports [12,17,19,21].

The results of the spectroscopic gap measurement discussed above are indeed similar to what was shown in Ref. [23] for disordered InO films. It was reported that disorder leads to the formation of preformed Cooper pairs with anomalously large binding energy and shows pseudogap behavior above T_c in the scanning tunneling spectroscopy (STS) spectra. When the disorder is rather low, coherence peaks were observed, while they were absent for the highly disordered sample even below T_c. Thus the present samples of the 1UC FeSe/STO system likely correspond to the low-disorder samples in Ref. [23]. However, it should be noted that our samples are single crystalline films epitaxially grown on a well-defined surface and the situation is totally different to the
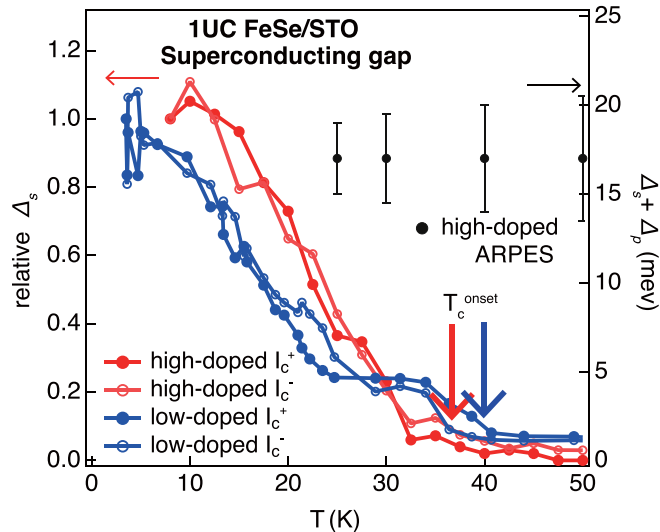
FIG. 4. Temperature dependence of the relative superconducting gap $\Delta_s(T)$ determined by $I_c^\pm$ of the 4PP and $\Delta_s + \Delta_p$ that includes the contribution of the preformed Cooper pair binding energy from ARPES measurements for the 1UC FeSe film grown on the high-doped STO, plotted together with that derived from $I_c^\pm$ for the 1UC FeSe film grown on the nondoped STO [11].

amorphous films in Ref. [23]. Thus there should be something that effectively acts as "disorder" in the 1UC FeSe/STO system. We believe that the STO surface is responsible for this, since the coherence length of the present system (1–2 nm) is nearly the same as the size of the $\sqrt{13} \times \sqrt{13}$ unit cell (1.4 nm) [24]. It was even shown that the local gap size can be different at different positions in the unit cell. Thus we can say that the electrons of the 1UC FeSe "feel" the potential of the STO surface to become preformed Cooper pairs at high temperatures since the energy scale to bind them is large, but at the same time are localized by the same potential. Thus it is likely that the gap measured with ARPES includes the contribution of the Cooper attraction energy between two electrons populating the same localized state $\Delta_p(T)$, as discussed in Ref. [23].

Figure 4 summarizes the key finding of the present work. As discussed above, $\Delta(T)$ derived from $I_c^\pm$ clearly showed temperature dependence below T_c^{onset} both for the samples grown on high-doped and low-doped STO substrates. This reflects the actual macroscopic global superconducting phenomena and thus we will call it $\Delta_s(T)$. In contrast, temperature-independent constant gap determined from the coherent peaks was observed in ARPES, which includes the effect of the preformed Cooper pairs presumably generated by the STO surface potential $[\Delta_s(T) + \Delta_p(T)]$. Thus it is clear that one needs to be aware of the definition of the "supercon-

ducting gap" measured in different experiments. It seems that although preformed Cooper pairs are present at a temperature as high as 60 K, they are localized and superconductivity does not occur. A similar statement concerning the difference between ARPES and transport data was made in Ref. [12]. It was suggested that incoherent Cooper pairs can form at temperatures much higher than the onset or the zero-resistance state due to the two dimensionality of this system. In addition, it was shown that although the actual disorder of the samples determined by the normal state resistance does affect T_c^{onset} or T_0 in this system, it is only a secondary factor for the incoherent pairing. This is in accordance to our statement that "disorder" in this system is actually the potential by the STO surface. We should also mention that there are cases where the strong disorder can inhibit the condensation of Cooper pairs without any spectroscopic evidence of a gap formation as clarified in disordered TiN [25]. Therefore, the correlation between reduced dimensionality, the actual disorder, and STO surface as well as their effect on the condensation or formation of Cooper pairs needs further investigation. Nevertheless, our work shows that interpretation of data based on spectroscopy techniques should be done carefully. It would be interesting to perform similar synchronous experiments on K-doped multilayer FeSe/STO, which has been shown to host high-T_c superconductivity [26].

IV. CONCLUSION

In conclusion, we have shown from *in situ* 4PP transport measurements that the superconducting properties of the 1UC FeSe/STO system do not depend on the doping level of the substrate, with $T_c^{onset} \sim 40$ K. The temperature dependence of the relative superconducting gap $\Delta_s(T)$ derived from the critical current increased by cooling down from T_c^{onset}. From *in situ* ARPES measurements, it was shown that the coherence peak develops at 60 K, whereas the Fermi level leading edge shift occurs below 40 K. We speculate that preformed Cooper pairs are formed due to the effect of the STO surface superstructure and its binding energy $\Delta_p(T)$ is measured together in ARPES.

[1] D. B. Haviland, Y. Liu, and A. M. Goldman, Phys. Rev. Lett. **62**, 2180 (1989).

[2] K. Ienaga, T. Hayashi, Y. Tamoto, S. Kaneko, and S. Okuma, Phys. Rev. Lett. **125**, 257001 (2020).

[3] T. Zhang, P. Cheng, W.-J. Li, Y.-J. Sun, G. Wang, X.-G Zhu, K. He, L. Wang, X. Ma, X. Chen *et al.*, Nat. Phys. **6**, 104 (2010).

[4] T. Uchihashi, P. Mishra, M. Aono, and T. Nakayama, Phys. Rev. Lett. **107**, 207001 (2011).

[5] M. Yamada, T. Hirahara, and S. Hasegawa, Phys. Rev. Lett. **110**, 237001 (2013).

[6] Y. Saito, Y. Kasahara, J. Ye, Y. Iwasa, and T. Nojima, Science **350**, 409 (2015).

[7] A. W. Tsen, B. Hunt, Y. D. Kim, Z. J. Yuan, S. Jia, R. J. Cava, J. Hone, P. Kim, C. R. Dean, and A. N. Pasupathy, Nat. Phys. **12**, 208 (2016).

[8] S. Yoshizawa, T. Kobayashi, Y. Nakata, K. Yaji, K. Yokota, F. Komori, S. Shin, K. Sakamoto, and T. Uchihashi, Nat. Commun. **12**, 1462 (2021).

[9] T. Sekihara, R. Masutomi, and T. Okamoto, Phys. Rev. Lett. **111**, 057005 (2013).

[10] J. F. Ge, Z. L. Liu, C. Liu, C. L. Gao, D. Qian, Q. K. Xue, Y. Liu, and J. F. Jia, Nat. Mater. **14**, 285 (2015).

[11] A. K. Pedersen, S. Ichinokura, T. Tanaka, R. Shimizu, T. Hitosugi, and T. Hirahara, Phys. Rev. Lett. **124**, 227002 (2020).

[12] B. D. Faeth, S. L. Yang, J. K. Kawasaki, J. N. Nelson, P. Mishra, C. T. Parzyck, C. Li, D. G. Schlom, and K. M. Shen, Phys. Rev. X **11**, 021054 (2021).

[13] J. Shiogai, Y. Ito, T. Mitsuhashi, T. Nojima, and A. Tsukazaki, Nat. Phys. **12**, 42 (2016).

[14] W. Qing-Yan, L. Zhi, Z. Wen-Hao, Z. Zuo-Cheng, Z. Jin-Song, L. Wei, D. Hao, O. Yun-Bo, D. Peng, C. Kai *et al.*, Chin. Phys. Lett. **29**, 037402 (2012).

[15] See Supplemental Material at http://link.aps.org/supplemental/10.1103/PhysRevMaterials.6.124801 for details on the annealing dependence of the APRES spectra, the Fermi level determination in ARPES, and the symmetrized analysis of the ARPES spectra for the inner band at the M point.

[16] M. Yamada, T. Hirahara, R. Hobara, S. Hasegawa, H. Mizuno, Y. Miyatake, and T. Nagamura, e-J. Surf. Sci. Nanotechnol. **10**, 400 (2012).

[17] S. He, J. He, W. Zhang, L. Zhao, D. Liu, X. Liu, D. Mou, Y.-B. Ou, Q.-Y. Wang, Zhi Li *et al.*, Nat. Mater. **12**, 605 (2013).

[18] Y. Hu, Y. Xu, Y.-M. Zhang, Q. Wang, S. He, D. Liu, A. Liang, J. Huang, C. Li, Y. Cai *et al.*, Phys. Rev. B **102**, 115144 (2020).

[19] S. Tan, Y. Zhang, M. Xia, Z. Ye, F. Chen, X. Xie, R. Peng, D. Xu, Q. Fan, H. Xu *et al.*, Nat. Mater. **12**, 634 (2013).

[20] V. Ambegaokar and A. Baratoff, Phys. Rev. Lett. **10**, 486 (1963); **11**, 104(E) (1963).

[21] Y. Xu, H. Rong, Q. Wang, D. Wu, Y. Hu, Y. Cai, Q. Gao, H. Yan, C. Li, C. Yin *et al.*, Nat. Commun. **12**, 2840 (2021).

[22] T. Kondo, W. Malaeb, Y. Ishida, T. Sasagawa, H. Sakamoto, T. Takeuchi, T. Tohyama, and S. Shin, Nat. Commun. **6**, 7699 (2015).

[23] B. Sacépé, T. Dubouchet, C. Chapelier, M. Sanquer, M. Ovadia, D. Shahar, M. Feigel'man, and L. Ioffe, Nat. Phys. **7**, 239 (2011).

[24] W. Si, T. Tanaka, S. Ichinokura, and T. Hirahara, Phys. Rev. B **105**, 104502 (2022).

[25] K. Bastiaans, D. Chatzopoulos, J. Ge, D. Cho, W. Tromp, J. van Ruitenbeek, M. Fischer, P. de Visser, D. Thoen, E. Driessen, T. Klapwijk, and M. Allan, Science **374**, 608 (2021).

[26] Y. Miyata, K. Nakayama, K. Sugawara, T. Sato, and T. Takahashi, Nat. Mater. **14**, 775 (2015).